

PCCP

Accepted Manuscript



This is an *Accepted Manuscript*, which has been through the Royal Society of Chemistry peer review process and has been accepted for publication.

Accepted Manuscripts are published online shortly after acceptance, before technical editing, formatting and proof reading. Using this free service, authors can make their results available to the community, in citable form, before we publish the edited article. We will replace this *Accepted Manuscript* with the edited and formatted *Advance Article* as soon as it is available.

You can find more information about *Accepted Manuscripts* in the [Information for Authors](#).

Please note that technical editing may introduce minor changes to the text and/or graphics, which may alter content. The journal's standard [Terms & Conditions](#) and the [Ethical guidelines](#) still apply. In no event shall the Royal Society of Chemistry be held responsible for any errors or omissions in this *Accepted Manuscript* or any consequences arising from the use of any information it contains.



PCCP

PAPER

Substrate effects on Li⁺ electrodeposition in Li secondary batteries with a competitive kinetics model

Received 00th January 20xx,
Accepted 00th January 20xx

Qian Xu, Yifu Yang*, Huixia Shao

DOI: 10.1039/x0xx00000x

www.rsc.org/pccp

Li₂₂Sn₅ alloy was prepared as a novel substrate of Li⁺ deposition for the metallic Li anode of rechargeable Li batteries. The performance of this alloy substrate was compared with those of Li, Cu, and Sn substrates. The deposition–stripping cycling performance of Li on the substrates was studied through galvanostatic charge–discharge method and cyclic voltammetry. The morphologies of the substrates before and after Li⁺ deposition were investigated through scanning electron microscopy and digital video microscopy. The electrochemical kinetics of Li⁺ electrodeposition on the different substrates was studied through galvanostatic pulse method and linear sweep voltammetry. The solid electrolyte interface films of Li deposits on the substrates were characterized through electrochemical impedance spectroscopy. Results show that Li₂₂Sn₅ is an excellent substrate for metallic Li electrodes. “The competitive kinetics model” was proposed as a novel mechanistic model to explain the electrodeposition behavior of Li⁺ on general substrates on the basis of electrochemical kinetics principles.

1. Introduction

The rapid development of electronic devices has led to an urgent demand for light power sources that employ high-energy-density materials. Li has long been considered as an anode for next-generation electrochemical energy storage systems because of its outstanding characteristics, such as low redox potential (−3.04 V vs. standard hydrogen electrode), high theoretical specific capacity (3860 mAh g^{−1}), and low density (0.59 g cm^{−3}).^{1–2} Nowadays, with the emergence of Li–S^{3–5} and Li–air^{6–8} batteries, metallic lithium anode has attracted considerable attentions.^{9–15}

However, the safety and cycle of metallic Li rechargeable batteries still need to be improved before these devices can be commercialized.¹⁶ The growth of Li dendrites during deposition and stripping cycles may lead to internal short circuit and incur fire or other safety problems.¹⁷ Therefore, researchers focused on restricting Li dendrite growth.^{18–20} It has been well known that the formation of Li dendrites is caused by various factors, such as inappropriate substrate, unsuitable electrolyte system and excess deposition current density, etc.²¹ All these factors will produce interaction and mutual influence on Li⁺ deposition. So solving the Li dendrite problem is a complex and systematic work. It is not likely to solve this problem only by one of the countermeasures. Only when a suitable substrate has been found, matched with an appropriate electrolyte system and being worked at a moderate deposition current density, can an uniform deposit of multi-layer Li deposition be obtained.

The inhomogeneous deposition of Li⁺ on substrates is a key factor

that triggers Li dendrite growth. Xu reported that the types and surface states of substrates influence the features of Li deposition.²² Li⁺ deposition is generally a layer-by-layer process. The quality of the first layer deposit has significant impact on the following multilayer deposition of lithium. The function of substrates is to form the first layer of Li deposit with excellent uniformity. Li easily reacts with many organic electrolytes, indicating that this metal is not a favorable substrate. Hence, the identification of novel suitable substrates to replace pure metallic Li for Li anodes is crucial. Li alloys with Sn, Ni, Sb, Si, Mg, and Al have been widely studied as Li storage materials for metallic Li rechargeable batteries.^{23–32} However, these alloys suffer from volume expansion and pulverization during charge–discharge cycling, which results in rapid capacity fading. Alloy elements can weaken the reactivity of Li with electrolytes and suppress the formation of Li dendrites. Thus, Li-containing alloys are potential substitute substrates to Li storage materials for Li electrodes. Therefore, finding a suitable substrate is an effective way to solve the problem related to Li dendrite growth and to improve Li resource utilization.

Considering the abovementioned findings, we selected Li₂₂Sn₅ alloy as a candidate substrate for Li⁺ deposition in the present study. This alloy demonstrates satisfactory cycling performance and excellent surface morphological characteristics. Meanwhile, “the competitive kinetics model” was proposed and demonstrated as a novel mechanistic model. This model was used to explain Li⁺ electrodeposition on general substrates.

2. Experimental

2.1 Preparation of Sn substrate precursor

College of Chemistry and Molecular Sciences, Wuhan University, Wuhan, P.R. China
Corresponding author, Tel.: +86 27 68756765; fax: +86 27 68754067.
E-mail address: yang-yf1@vip.sina.com (Y. F. Yang).

Sn was selected as the initial substrate precursor, and it was prepared via electrodeposition on a Cu electrode from an aqueous solution that contains $0.175 \text{ mol L}^{-1} \text{ SnCl}_2 \cdot 2\text{H}_2\text{O}$, $1 \text{ mol L}^{-1} \text{ F}_2\text{H}_5\text{N}$, 0.1 mol L^{-1} citric acid, 2 g L^{-1} polyethylene glycol, and 2 g L^{-1} hydroquinone. The pH of the solution was maintained at 5.0 to 7.0. The Cu electrode was prepared with a rounded Cu rod wrapped in a polytetrafluoroethylene rod, and the surface of the Cu electrode was polished smoothly and cleaned with ultrapure water before Sn electrodeposition. The electrodeposition of Sn on Cu was performed at current density of $10 \text{ mA} \cdot \text{cm}^{-2}$ for 30 min at $30 \text{ }^\circ\text{C}$, and ultrasonication was adopted throughout the electrodeposition process.

2.2 Preparation of Li–Sn alloy substrate

Li and Sn can form various alloy forms, such as Li_2Sn_5 , Li_5Sn_2 , and Li_7Sn_3 ,³³ among these alloys, $\text{Li}_{22}\text{Sn}_5$ has the largest Li molar ratio. Different alloys are formed with different deposition potentials; among these alloys, $\text{Li}_{22}\text{Sn}_5$ is formed between 0.38 and 0 V (vs. Li/Li^+). When the deposition potential reaches 0 V at a low current density, the Li content in the Li–Sn alloy reaches a saturated state; moreover, a metallic Li phase is formed on the alloy surface as deposition continues. In this process, the alloy status is defined as 100% Li ($C_{\text{Li}} = 100\%$) when the deposition potential reaches 0 V. Previous experiments confirmed that 20,000 s is needed to reach 0 V under our preset experimental conditions. Thus, $C_{\text{Li}} = 20\%$, $C_{\text{Li}} = 40\%$, $C_{\text{Li}} = 60\%$, $C_{\text{Li}} = 80\%$, and so on can be obtained by assuming that Li^+ deposition is time homogeneous. This experiment was operated with a specially designed electrolytic cell and assembled in an Ar gas-filled glove box (Etelux Lab2000, China). The electrolyte was a $1 \text{ mol L}^{-1} \text{ LiClO}_4/\text{ethylene carbonate (EC) + dimethyl carbonate (DMC)}$ (1:1 vol. %) solution.

2.3 Morphological determination

The surface morphologies of the substrates and Li deposits were analyzed under a scanning electron microscope (SEM, ZEISS Merlin Compact, Germany) and a 3D digital microscope (VHX-2000, Keyence Corporation, Japan).

2.4 Electrochemical measurements

Galvanostatic charge and discharge cycling experiments were conducted using a CT2001A Battery Tester (Land Electronic Equipments Company, China) at $25 \text{ }^\circ\text{C}$. The polarization curves of Li^+ deposition on the substrates were drawn and cyclic voltammetry (CV) was performed in a three-electrode cell using Li foil as the counter and reference electrodes with a CHI 611b Electrochemical Workstation (Chenhua, China) at a scan rate of 5 mV s^{-1} . Electrochemical impedance spectroscopy was conducted with Reference 600 Potentiostat (GAMRY Instruments, USA) at a frequency range of 100 kHz to 0.01 Hz.

3. Results and discussion

3.1 Characteristics of Li deposition on the $\text{Li}_{22}\text{Sn}_5$ substrate

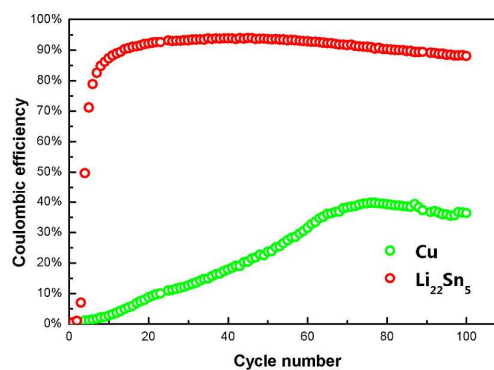


Fig. 1 Relationship of Coulombic efficiencies with cycle number of Li^+ deposition on the $\text{Li}_{22}\text{Sn}_5$ and Cu substrates. Counter electrode: Li foil; electrolyte: $1 \text{ mol L}^{-1} \text{ LiClO}_4/\text{EC} + \text{DMC}$.

The deposition–stripping cycle performance of Li on the $\text{Li}_{22}\text{Sn}_5$ and Cu substrates were tested and compared. In each cycle, Li was first deposited on the substrates at a current density of 0.1 mA cm^{-2} for 1000 s. Afterward, the deposited Li was oxidized at the same current density until the potential reached the cut-off value. To ensure that the cycling procedure exclusively comprised Li deposition–stripping on the surface of the $\text{Li}_{22}\text{Sn}_5$ substrate but not alloying and de–alloying, the cut-off potential of Li oxidation on the $\text{Li}_{22}\text{Sn}_5$ substrate was set as 0.3 V. The cut-off potential of Li oxidation on the Cu substrate was set as 3.0 V to ensure that the deposited Li can be thoroughly oxidized. Fig. 1 shows the relationship of the coulombic efficiency with the cycle number of Li^+ deposition on the $\text{Li}_{22}\text{Sn}_5$ and Cu substrates. The cycling performance significantly differed on the different substrates. The Li^+ deposition–stripping cycling performance significantly improved when $\text{Li}_{22}\text{Sn}_5$ was used as the substrate. Moreover, the Coulombic efficiency was still as high as 90% after 100 cycles. By contrast, the Coulombic efficiency of Li^+ deposition on the Cu substrate was lower than 40% after similar cycles. There are some very low coulombic efficiency appears in the initial several cycles of the $\text{Li}_{22}\text{Sn}_5$ substrate, because in the formation process of Li–Sn alloys, the deposition potential of Li^+ is relatively high and the formation speed of Li–Sn alloy may be quicker than that of the formation of solid electrolyte interface (SEI) film. Due to these reasons, the formation of an effective SEI film is not well finished during the formation of Li–Sn alloys. But when Li^+ deposit on $\text{Li}_{22}\text{Sn}_5$ substrate, some of the newly formed Li metal atoms will react with the electrolyte, which can consume the Li metal atoms and reduce the coulombic efficiency. In general, a functional SEI film is formed in a few cycles of lithium plating and stripping due to the low formation speed of the SEI film. But Cu metal is not a suitable substrate for the uniform deposition of Li^+ . As a result Li-ions are preferred to deposit on the surface of the previously deposited lithium particles, but not on the Cu substrate. This situation is easy to lead to the uncontrollable growth of the Li particles and the formation of Li dendrites. SEI film can also be formed on the surface of the dendrites, as the dendrites are broken, the insulating feature of the SEI film on the broken dendrite can isolate them from the bulk of the lithium particles or the substrate. This has caused a great reduction of the coulombic efficiency of lithium plating and stripping on Cu substrate. Such a

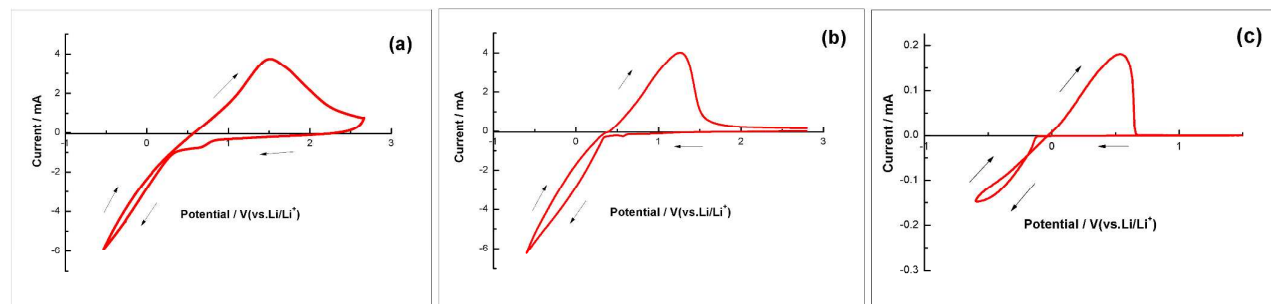


Fig. 2 CV curves of Li deposition and stripping on different substrates. (a) $\text{Li}_{22}\text{Sn}_5$; (b) Sn; (c) Cu. Counter and reference electrodes: Li foil; electrolyte: $1 \text{ mol L}^{-1} \text{ LiClO}_4/\text{EC} + \text{DMC}$.

case is not improved along with the cycling, so the coulombic efficiency of lithium deposition on Cu is kept low in the whole process of cycling. Meanwhile, the amount of deposited Li particles is increased gradually, so that more lithium can be plated and stripped, this can result in a relatively higher coulombic efficiency. So for the Cu substrate, the coulombic efficiency keeps increasing upon cycling.

Fig. 2 compares the CV curves of Li deposition–stripping on the $\text{Li}_{22}\text{Sn}_5$, Sn, and Cu substrates. This figure shows that the Li^+ deposition on the $\text{Li}_{22}\text{Sn}_5$ alloy and Sn substrates were “underpotential”; therefore, the starting potential of Li^+ deposition was higher than 0 V (vs. Li/Li^+). However, the Li^+ deposition on the Cu substrate was “overpotential”; therefore, the starting potential of Li^+ deposition on Cu was lower than 0 V (vs. Li/Li^+) because Li cannot form an alloy with Cu.

Fig. 3 compares the surface morphologies of the Cu, Li, and $\text{Li}_{22}\text{Sn}_5$ substrates before and after Li^+ deposition at a current density of 0.1 mA cm^{-2} for 1000 s. Figs. 3(a) and 3(b) show that the surface of the $\text{Li}_{22}\text{Sn}_5$ substrate was smooth before Li deposition and that no dendrites formed after Li deposition. Fig. 3(c) and 3(d) compare the surfaces of the Li foil before and after Li deposition, respectively. Apparently, dendrites generated and spread on the surface of the Li foil. By contrast, granular and isolated Li obviously formed after Li deposition on the Cu substrate as compared with its original state before Li deposition [Fig. 3(e) and 3(f)].

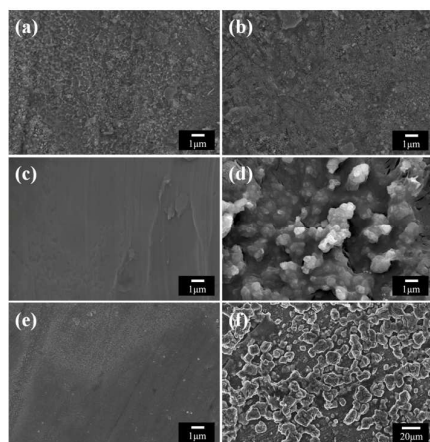


Fig. 3 SEM images of different substrates before and after Li deposition for 1000 s at a current density of 0.1 mA cm^{-2} . (a) $\text{Li}_{22}\text{Sn}_5$; (b) $\text{Li}_{22}\text{Sn}_5$ after Li deposition; (c) Li; (d) Li after Li deposition; (e) Cu; and (f) Cu after Li deposition. Electrolyte: $1 \text{ mol L}^{-1} \text{ LiClO}_4/\text{EC} + \text{DMC}$.

In this study, 1000 seconds is just an artificially set time, but not the critical time for the first layer deposition. In fact, it is very difficult to determine the electric quantity that the first-layer deposition requires, because the Li–Sn alloy substrate itself is not an ideal smooth surface and the actual superficial area is difficult to be determined. In another aspect, our final research target is the uniform multilayer deposition of lithium, but not the mechanism of the first layer formation, it is not necessary to strictly control the electric quantity to guarantee lithium deposit is in a single layer. That is to say, 1000 seconds of deposition may correspond to multilayer deposition. In addition, the situation of Li deposition for longer time has also been studied at the same time. The SEM images of $\text{Li}_{22}\text{Sn}_5$ substrate after Li deposition for 2000 seconds and even longer time show that the electrode surfaces remain relative smooth and no Li dendrites have been observed. These results are not shown in this paper, just because for contrast purpose, the deposition time of all the experiments were set as 1000 seconds.

3.2 Competitive kinetics model of Li deposition on general substrates

The results above clearly indicate that $\text{Li}_{22}\text{Sn}_5$ is an ideal substrate for Li^+ deposition with excellent uniformity and favors Li deposition–stripping cycling. Therefore, a thorough understanding of the mechanism is expected. Several meaningful and fundamental models concerning the mechanism of Li dendrite formation have been proposed in the last 40 years. Examples of these models include the “surface–tension model” proposed by Barton and Bockris in the 1960s,^{34–37} the “Brownian statistical simulation model” in the 1980s,^{38–42} the “Chazalviel electro-migration–limited model” developed in the 1990s,^{43–47} and Yamaki’s theory in the 1990s.⁴⁸ These mechanistic models explain specific situations from different perspectives, with respective superiorities but also limitations. In the current work, we proposed and demonstrated the “competitive kinetics model” as a novel mechanistic model to explain the electrodeposition of Li^+ on general substrates on the basis of electrochemical kinetics principles.

Li^+ deposition occurs on a substrate M (except Li); thus, the deposited Li initially forms particle–like aggregation. For simplicity of expression, this process is named as initialization stage in the current work. This process is schematically illustrated in Fig. 4. After initialization, two types of interactions immediately occur. One is the interaction between Li^+ and the surface atoms of M

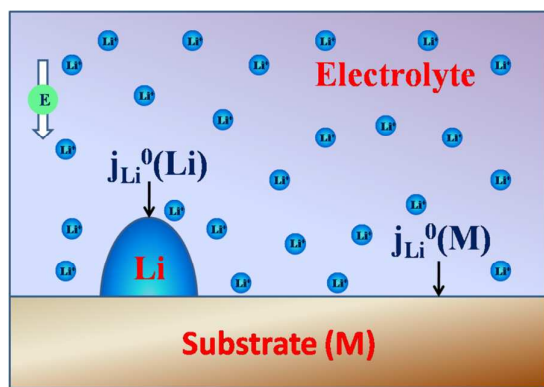


Fig. 4 Schematic of Li^+ deposition on M substrate.

substrate. The other is the interaction between Li^+ and the metallic Li atoms of the deposited Li particles on M substrate.

Therefore, two substrates (Li metal and M substrates) are combined in this system. Hence, subsequent Li^+ deposition occurs either on Li metal or on M substrate depending on the competitive relationship between the Li deposition reactions on these two substrates. This competition is in fact the key in determining the morphology of Li^+ deposits.

The competitive relationship of Li deposition on the Li substrate, the M substrate, or both is determined by two main factors. One is the comparative relationship of exchange current density. We can define $j_{\text{Li}}^0(\text{Li})$ and $j_{\text{Li}}^0(\text{M})$ as the exchange current density of Li^+ deposition and oxidation reactions on the Li and M substrates, respectively. The other is the comparative relationship of the electrode potential at which Li^+ deposition is initiated on the substrates. We can also define $\phi_{\text{Li}}^0(\text{M})$ as the starting potential of Li^+ deposition on M substrate (excluding Li metal) and $\phi_{\text{Li}}^0(\text{Li})$ as the substrate on Li metal. On the basis of these definitions, “the competitive kinetics model” was proposed as a new mechanistic model of Li^+ electrodeposition on general substrates. Fig. 5 shows the schematic of the polarization curves of Li^+ deposition on both the Li and M substrates, in which the abscissa and ordinate represent the negative potential ($-\phi$) and the cathodic current density (j_c), respectively. The “Li” and “M” on the curves represent the corresponding substrates. Four situations can be classified in accordance with the comparative relations of these two factors.

(1) When $j_{\text{Li}}^0(\text{Li}) \geq j_{\text{Li}}^0(\text{M})$ and $-\phi_{\text{Li}}^0(\text{Li}) \leq -\phi_{\text{Li}}^0(\text{M})$ [Fig. 5(a)], the polarization of Li^+ deposition on the Li substrate is lower than that on the M substrate, and the starting potential of Li^+ deposition is more positive on the Li substrate than on M substrate. As a result, these two polarization curves do not intersect at any time. When $-\phi_{\text{Li}}^0(\text{Li}) < -\phi_c < -\phi_{\text{Li}}^0(\text{M})$, the whole current is contributed by Li^+ deposition on the Li substrate; therefore, Li particles gradually develop. When $-\phi_c > -\phi_{\text{Li}}^0(\text{M})$, the cathodic current is composed of Li^+ deposition on both the Li and M substrates with $j_c(\text{Li}) > j_c(\text{M})$ at the same potential. As a result, Li^+ tends to deposit on the Li substrate. This condition promotes Li dendrite growth.

(2) When $j_{\text{Li}}^0(\text{Li}) \geq j_{\text{Li}}^0(\text{M})$ and $-\phi_{\text{Li}}^0(\text{Li}) \geq -\phi_{\text{Li}}^0(\text{M})$ [Fig. 5(b)], the two polarization curves intersect at point B, which corresponds to a potential $-\phi_B$ at which the current density of Li^+ deposition is

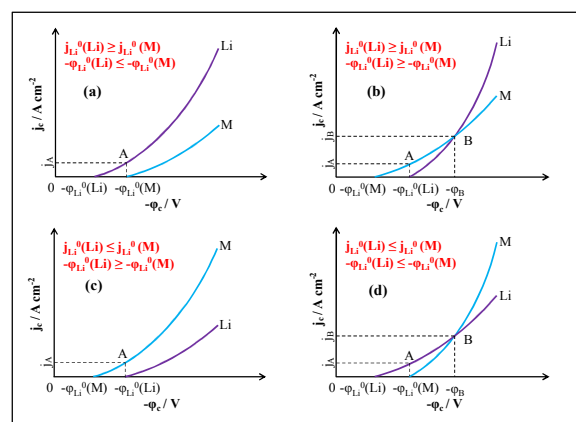


Fig. 5 Schematic of the competitive relationships of Li^+ deposition on the Li and M substrates.

equal on the Li and M substrates. The entire curve can be divided into three sections. The first section is within the potential range of $-\phi_{\text{Li}}^0(\text{M}) < -\phi_c < -\phi_{\text{Li}}^0(\text{Li})$; within this range, the cathodic current solely originates from Li^+ deposition on the M substrate, and a uniform morphology of Li deposits is the only possibility. The second section is within the potential range of $-\phi_{\text{Li}}^0(\text{Li}) < -\phi_c < -\phi_B$; within this range, the cathodic current originates from Li^+ deposition on both the Li and M substrates, in which the latter one is the main contributor because of the higher current density on the M substrate and higher surface area of the M substrate than on the Li deposit. This finding is conducive to the homogeneous Li^+ deposition on the M substrate. The third section is within the potential range of $-\phi_B < -\phi_c$; within this range, the cathodic current originates from Li^+ deposition on both the Li and M substrates when $j_{\text{Li}}^0(\text{Li}) \geq j_{\text{Li}}^0(\text{M})$. This condition benefits the formation of Li dendrites because of the high current density of Li^+ deposition on the Li substrate.

(3) $j_{\text{Li}}^0(\text{Li}) \leq j_{\text{Li}}^0(\text{M})$ and $-\phi_{\text{Li}}^0(\text{Li}) \geq -\phi_{\text{Li}}^0(\text{M})$ [Fig. 5(c)] is an ideal situation for uniform Li^+ deposition on the M substrate. Within the potential range of $-\phi_{\text{Li}}^0(\text{M}) \leq -\phi_c \leq -\phi_{\text{Li}}^0(\text{Li})$, the cathodic current only originates from Li^+ deposition on M. When $-\phi_c \geq -\phi_{\text{Li}}^0(\text{Li})$, the cathodic current is contributed by Li^+ deposition on both the Li and M substrates, in which the latter is dominating. In such a case, Li dendrites are not easily formed.

(4) When $j_{\text{Li}}^0(\text{Li}) \leq j_{\text{Li}}^0(\text{M})$ and $-\phi_{\text{Li}}^0(\text{Li}) \leq -\phi_{\text{Li}}^0(\text{M})$ [Fig. 5(d)], two polarization curves intersect at potential $-\phi_B$, at which the current density of Li^+ deposition is equal on both the Li and M substrates. The entire curve can be divided into three sections similar to that in Fig. 5(b). The first section is within the potential range of $-\phi_{\text{Li}}^0(\text{Li}) \leq -\phi_c \leq -\phi_{\text{Li}}^0(\text{M})$; within this range, Li deposition can only occur on Li. However, at this stage, no Li particles form on the M substrate before initialization; therefore, this result is within the potential range with the current equal to zero. The second section is within the potential range of $-\phi_{\text{Li}}^0(\text{M}) \leq -\phi_c \leq -\phi_B$; within this range, as Li^+ deposition starts on the M substrate, newly formed Li particles function as the new substrate. Moreover, Li^+ deposition is preferred on this new substrate. The third section is within the potential range of $-\phi_B \leq -\phi_c$; within this range, Li^+ deposition on

the M substrate becomes dominating. This condition benefits the formation of Li^+ deposits with a uniform morphology.

On the basis of the abovementioned principles, the uniformity of Li^+ deposition strongly depends on the competitive relationship between the reaction of Li^+ deposition on the M and Li substrates because the effects of the nonuniformity of the solid electrolyte interface (SEI) are ignored. To verify the rationality of this model, the first step is to obtain the exchange current density data of Li^+ deposition on different substrates. As a key electrochemical kinetics parameter, the exchange current density (j^0) is defined as the absolute cathodic and anodic current density when the electrode reaction reaches equilibrium. A high j^0 value indicates that simultaneous oxidation and reduction reactions occur at a high speed with a relatively low polarization.

When the polarization overpotential is adequately small (i.e., < 25 mV), the relationship of the current density with overpotential can be expressed as

$$\eta = -\frac{RT}{j_0 n F} j \quad (1)$$

where η represents overpotential, j represents the actual current density, j_0 is the exchange current density, n is the number of transferred electron, F is Faraday's constant, R is the gas constant, and T is the absolute temperature (298.15 K). Thus, the exchange current density (j_0) can be calculated using the slope of the linear relationship between η and j .

The potential changes with time when a current pulse is used to trigger Li^+ deposition, and the influence of mass transference can be ignored if time is adequately short. Furthermore, the potential can achieve low polarization and slow change rate when the current density is adequately small. Consequently, the charging effect of double-layer capacitance can also be ignored.

Therefore, a relative η value can be obtained at a certain time with a definite current density. Changing the current pulse can yield a set of data couples of η with current density j and demonstrate a linear relation of η versus j .

In the present study, an open circuit potential (ϕ_{oc}) was recorded when the potential stabilized before Li deposition on a specific substrate. Afterward, Li^+ deposition occurred for 1 s at different current densities. The deposited Li was stripped for 1 s at the same current density immediately after pulse deposition to ensure that the electrode recovered to its initial conditions. The testing current density ranged from $0.01 \mu\text{A cm}^{-2}$ to $200 \mu\text{A cm}^{-2}$. The time interval of data sampling was set to 0.002 s. Afterward, the first potential value ϕ was recorded as reaction potential; thus, η can be calculated as

$$\eta = \phi_{oc} - \phi_c \quad (2)$$

The measured η - j relationship that corresponds to different substrates is shown in Fig. 6. As aforementioned, when the polarization overpotential (η) is small enough, η shows a linear relationship to the actual current density (j), and the slope $[S(M)]$ of the straight line relating to the different substrates varies. The sequence was $S(\text{Li}) < S(\text{Sn}) < S(\text{Cu})$ among these three substrates. In another aspect, $S(\text{Li}_{22}\text{Sn}_5)$ has the lowest value among all of the Li-Sn alloys with different C_{Li} values. The exchange current densities of Li^+ deposition on the different substrates were calculated on the basis of the linear fitting relationships. The calculation results in Table 1 show that the j_0 of Li reactions is extremely greater on the $\text{Li}_{22}\text{Sn}_5$ substrate than on the Cu and Sn substrates. However, the j_0 of Li reactions on the $\text{Li}_{22}\text{Sn}_5$ substrate is still slightly less than that on the Li substrate.

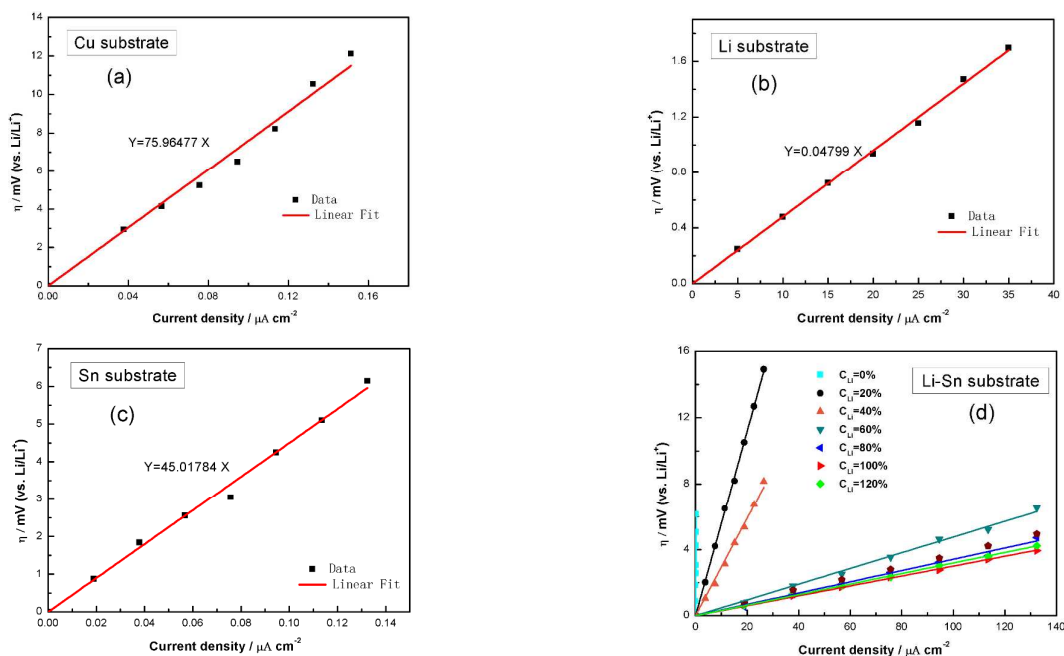


Fig. 6 Relationships of the overpotential of Li deposition with current density on different substrates. (a) Cu; (b) Li; (c) Sn; (d) Li-Sn alloy with different C_{Li} values.

Table 1 Data of j_0 for different substrates

Substrate	$j_0 / \text{mA cm}^{-2}$
$C_{\text{Li}} = 0$ (Sn)	0.0006
$C_{\text{Li}} = 20\%$	0.0230
$C_{\text{Li}} = 40\%$	0.0436
$C_{\text{Li}} = 60\%$	0.2697
$C_{\text{Li}} = 80\%$	0.3765
$C_{\text{Li}} = 100\%$	0.4286
$C_{\text{Li}} = 120\%$ ^①	0.4031
Cu	0.0003
Li	0.5354

① $C_{\text{Li}} = 120\%$ represents continued Li^+ deposition for a specified time on the Li–Sn alloy substrate after reaching $C_{\text{Li}} = 100\%$.

As shown in Fig. 8, the relationship of the exchange current density is $j_{\text{Li}}^0(\text{Cu}) < j_{\text{Li}}^0(\text{Sn}) < j_{\text{Li}}^0(\text{Li})$ in accordance with the changing trends of the three polarization curves. Moreover, the Li^+ deposition on the Sn substrate is “underpotential,” whereas that on the Cu substrate is “overpotential.” This finding is generally consistent with the CV experimental results. The performance of Li^+ deposition on the different substrates (e.g., Cu, Sn, and Li–Sn alloy) can be predicted on the basis of the exchange current density and the starting potential of Li^+ deposition on the substrates. When Li^+ deposition occurs on the Cu substrate, $\phi_{\text{Li}}^0(\text{Li})$ is relatively more positive than $\phi_{\text{Li}}^0(\text{Cu})$, and the cathodic current density of Li^+ deposition is higher on the Li substrate than on the Cu substrate throughout cathodic polarization. This condition benefits the formation of Li dendrites. Unlike the polarization curve of Li^+ deposition on the Cu substrate, that on the Li–Sn substrate can be divided into the following parts. When the potential is within the range of $\phi_{\text{Li}}^0(\text{Li}) \leq \phi_c \leq \phi_{\text{Li}}^0(\text{Sn})$, the cathodic current is solely contributed by Li^+ deposition on the Li–Sn substrate accompanied by alloy formation; this condition benefits

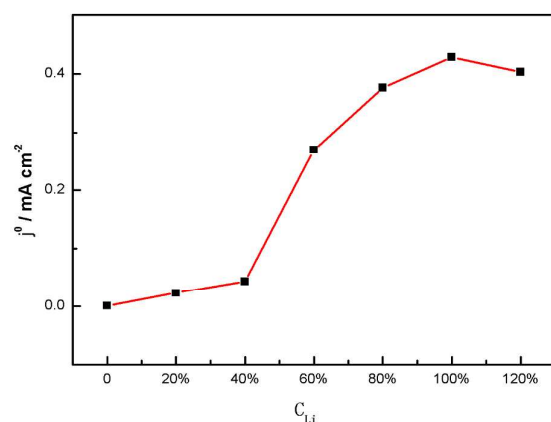


Fig. 7 Exchange current densities of Li^+ deposition on the Li–Sn substrates with different C_{Li} values.

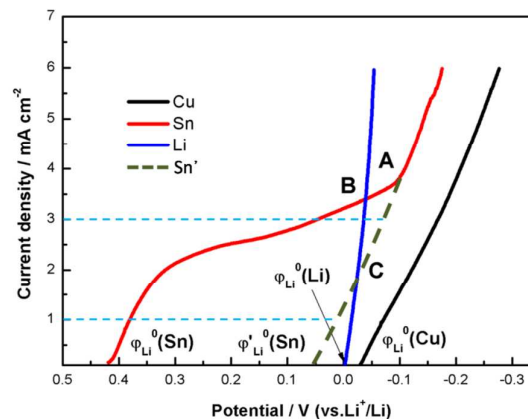


Fig. 8 Polarization curves of Li^+ deposition on M substrate (M = Cu, Sn, Li).

the uniform deposition of Li. When the potential is within the range of $\phi_{\text{Li}}^0(\text{Li}) < \phi_c < \phi_{\text{Li}}^0(\text{Sn})$, Li deposition on the surface of the $\text{Li}_{22}\text{Sn}_5$ alloy should have an expected uniform morphology. When the potential is within the range of $\phi_c < \phi_{\text{Li}}^0(\text{Li})$, the cathodic current is contributed by Li deposition on the surface of both the Li and $\text{Li}_{22}\text{Sn}_5$ substrates. This condition may be observed during Li dendrite growth but at a relatively low speed. Current density is the key parameter controlling the potential of Li deposition. Therefore, Li deposits can be uniformly formed at a relatively low current density [i.e., when $\phi_c > \phi_{\text{Li}}^0(\text{Li})$].

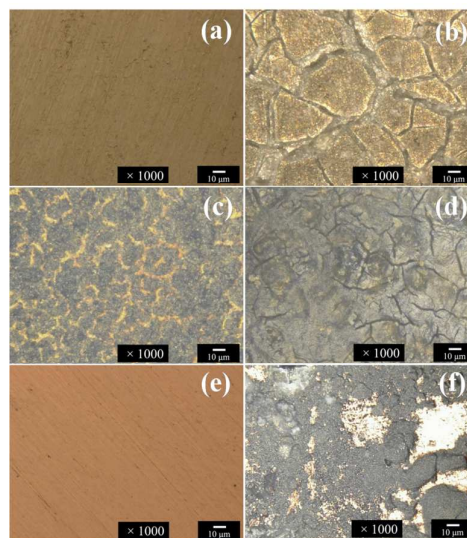


Fig. 9 Morphologies of different substrates. (a) Sn foil; (b) Li–Sn alloy after Li deposition until the potential reaches 0 V at the current density of 0.1 mA cm^{-2} ; (c) Li–Sn alloy after Li deposition at 3 mA cm^{-2} for 1000 s; (d) Li–Sn alloy after Li deposition at 1 mA cm^{-2} for 1000 s; (e) Cu before Li deposition; (f) Cu after Li deposition at 0.1 mA cm^{-2} for 1000 s. Electrolyte: $1 \text{ mol L}^{-1} \text{ LiClO}_4/\text{EC} + \text{DMC}$.

To verify the abovementioned hypothesis, images of Li deposits on different substrates were captured (Fig. 9). As shown in Fig. 9(a), the substrate of Sn foil was smooth before Li⁺ deposition. A Li–Sn alloy with various Li contents forms during Li⁺ deposition.³³ Li₂₂Sn₅ forms as the potential reaches 0 V with slight volume expansion [Fig. 9(b)]. This process is consistent with that when the potential is within the range of $\phi_{\text{Li}}^0(\text{Sn}) \sim \phi_{\text{A}}$ of the polarization curve on the Sn substrate in Fig. 8. When the deposition current density is set to 3 mA cm⁻², the cathodic current density is composed of Li⁺ deposits on both the Li and Li–Sn alloy substrates, with the former being the dominant substrate; therefore, Li⁺ tends to deposit on the Li substrate, which promotes Li dendrite growth [Fig. 9(c)]. However, when the deposition current density is set to 1 mA cm⁻², Li⁺ deposition on the Li–Sn alloy substrate dominates [Fig. 9(d)]. The morphology of the Cu substrate is observed before and after Li⁺ deposition [Figs. 9(e) and 9(f)]. $\phi_{\text{Li}}^0(\text{Cu}) < \phi_{\text{Li}}^0(\text{Li})$ within the entire range of cathodic current; thus, the cathodic current contributed by Li⁺ deposition on the Li substrate is higher than that on the Cu substrate. This condition benefits the formation of Li dendrites [Fig. 9(f)]. The morphology of Li deposits is more uniform on the Li–Sn substrate than on the Cu substrate at a suitable current density range. These results highly support the “competitive kinetics model.”

3.3 Characteristics of SEI film on the Li₂₂Sn₅ substrate

The influence of the SEI film is ignored in the “competitive kinetics model”. However, the nature and structure of the SEI film usually greatly influences the deposition behavior of Li⁺. Fig. 10(a) to 10(c) show the impedance curves (Nyquist plots) and equivalent circuits of the Li substrate, the Li–Sn substrates with different C_{Li} values, and the Cu substrate, respectively. As shown in Fig. 10(a), the features of the impedance curve in the high-frequency range are associated with the migration of Li⁺ in the SEI film, those of the curve in the mid-frequency range correspond to the Li⁺ charge transfer process at the SEI film–Li metal interface, and those of the curve in the low-frequency range are ascribed to Li⁺ diffusion in the electrolyte.⁴⁹ Fig. 10(b) shows the impedance spectrum of Li reaction on the Li–Sn alloy. When C_{Li} = 100% in the Li–Sn alloy, Li⁺ directly deposits on the Li–Sn alloy surface, and Li atoms no longer penetrate into the inner part of the Sn substrate. Therefore, the equivalent circuits of the Li–Sn substrates could be divided into two cases, namely, C_{Li} ≤ 100% and C_{Li} > 100%. When C_{Li} < 100%, the impedance spectrum shows that the semicircle diameter in the high-frequency range becomes increasingly smaller as the C_{Li}

continuously increases. When C_{Li} = 100%, this diameter reaches the minimum value. The two semicircles, or called two branch equivalent circuits may differ just a little and cannot be distinguished clearly, so two semicircles merge with each other, showing that only one asymmetrical semicycle is present in this situation. Furthermore, the impedance of the Li–Sn alloy reduces as C_{Li} increases and reaches 100%. However, upon Li₂₂Sn₅ formation, further Li⁺ deposition triggers the formation of the Li metal phase over the Li₂₂Sn₅ alloy. Moreover, the diameter of the semicircle on the impedance spectrum increases again. This result clearly indicates that the resistance for Li⁺ migration in the SEI film decreases when C_{Li} < 100% and increases again when C_{Li} > 100%. As a comparison, no semicircle can be observed in the high-frequency range of the impedance curve of the Cu substrate because the SEI film that formed on the Cu substrate is nonuniform and incomplete [Fig. 10(c)], for the semicircle is a criterion to judge the integrity of the SEI film, only when the SEI film is complete, can the SEI film be equal to the parallel connection of corresponding capacitance and resistance. However, when the SEI film is incomplete, it means that the electrode surface is not fully covered by SEI film, the situation becomes much more complex. In such a case the electrode-solution interface could be divided into two parts--- the interface between the electrode surface covered by SEI film and the solution, and the interface between the electrode surface without SEI film and the solution. These two types of interface are in parallel, anyone of them has its own independent equivalent circuit, which means independent connection of corresponding capacitance and resistance. In this situation, the response of the whole equivalent circuit to the EIS stimulation will not behave as semicircle. The diversity of the impedance curves can be attributed to the kinetics characteristics of Li⁺ deposition on the different substrates and the nature and structure of the SEI films.

For equivalent circuits, R_Ω is the overall resistance of the system, including the ohmic resistance of the solution and the resistance of the electrode itself. The constant-phase element Q_{SEI} represents the capacitance of the SEI film, and R_{SEI} represents the resistance of the SEI film. Q_d is the capacitance of the electrical double layer. R_{ct} is the charge transfer impedance. Q_w is the solid-phase diffusion impedance. Q_i and R_i represent the capacitance and resistance of the Li–Sn alloy layer, respectively. The impedance curves in Fig. 10 can be fitted in accordance with equivalent circuits, and parameter values can be obtained.

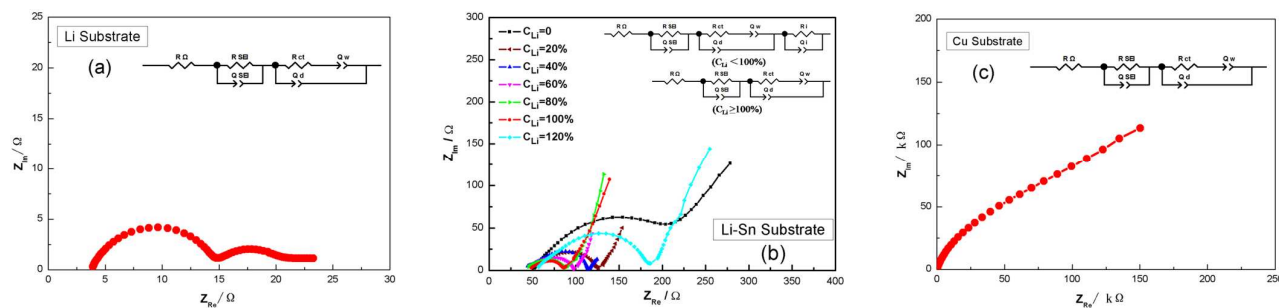


Fig. 10 Impedance diagrams of different substrates. (a) Li; (b) Li–Sn alloy with different C_{Li} values; (c) Cu.

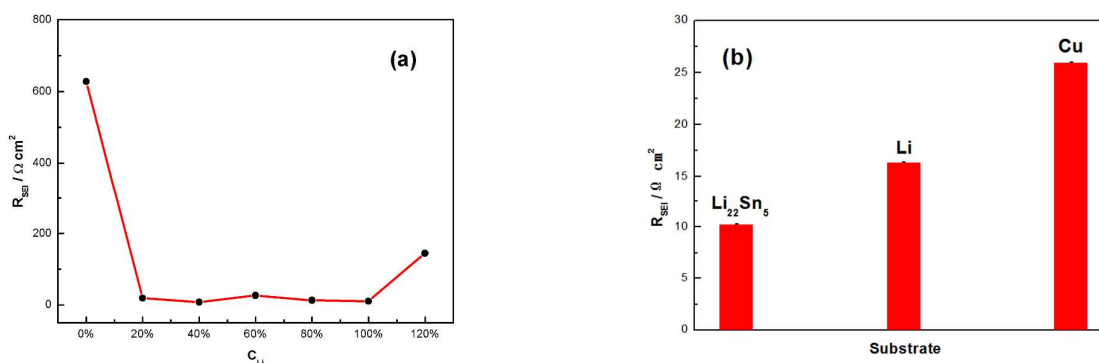


Fig. 11 Resistance of the SEI film of different substrates. (a) Li–Sn alloy with different C_{Li} values; (b) Comparison of the resistance of the SEI film of the $\text{Li}_{22}\text{Sn}_5$, Li, and Cu substrates.

The resistance of the SEI film (R_{SEI}) of different substrates is shown in Fig. 11 to characterize the Li–Sn alloy in detail. Fig. 11(a) compares the R_{SEI} values of the Li–Sn alloy with different C_{Li} values. R_{SEI} increases when the substrate is pure Sn but sharply reduces when the Li–Sn alloy is formed ($C_{Li} \leq 20\%$). When C_{Li} ranges from 20% to 100%, R_{SEI} is roughly relevant to the C_{Li} value. When $C_{Li} = 100\%$ ($\text{Li}_{22}\text{Sn}_5$), R_{SEI} reaches the minimum value of $10.25 \Omega \text{ cm}^2$. Fig. 11(b) compares the R_{SEI} values among the $\text{Li}_{22}\text{Sn}_5$, Li, and Cu substrates. This figure shows that $\text{Li}_{22}\text{Sn}_5$ has the least R_{SEI} among the three substrate systems. R_{SEI} can reflect the growth of the SEI film given that the components of the SEI film remain constant throughout the entire Li^+ deposition process. In particular, R_{SEI} positively correlates with SEI film thickness. Therefore, $\text{Li}_{22}\text{Sn}_5$ has the thinnest SEI film among all of the substrates used. Excessive SEI film thickness hinders Li^+ transportation between the electrolyte and the anode; this phenomenon affects uniform Li^+ deposition. Basing from these results, we can conclude that $\text{Li}_{22}\text{Sn}_5$ is a suitable substrate for Li^+ deposition in metallic Li rechargeable batteries.

4. Conclusions

This study investigated the possibility of using a novel $\text{Li}_{22}\text{Sn}_5$ alloy as the substrate of the metallic Li anode in Li rechargeable batteries. Experimental results indicate that $\text{Li}_{22}\text{Sn}_5$ is an excellent substrate material for Li^+ homogeneous deposition and favors Li deposition–stripping cycling.

“The competitive kinetics model” is a unique mechanistic model of Li^+ electrodeposition on general substrates. Electrochemical kinetics principles were used to analyze the mechanism of the Li–Sn alloy substrate for Li anode on the basis of this model. The following three conclusions can be drawn. First, Li^+ electrodeposition on the Sn substrate shows continuous changes in exchange current density and polarization impedance. Second, the Li content in the Li–Sn alloy greatly affects the kinetics of Li^+ electrodeposition. The Li–Sn alloy with the highest Li content is the most beneficial substrate among the different substrates used. Third, the Li^+ electrodeposition performance on the $\text{Li}_{22}\text{Sn}_5$

substrate is much better than that on the Li and Cu substrates. This study elucidates how to select the suitable substrate and deposition current density for the metallic Li anode of Li rechargeable batteries.

“The competitive kinetics model,” which was established on the basis of Li^+ electrodeposition on general substrates, may be applied in studies on metallic Li anode and other electrodeposition phenomena, such as deposition morphology in Li-ion batteries after Li deposition at the interface. This model may also be applied to screen suitable substrates for the electroplating industry.

Acknowledgements

This work is financially supported by the National Natural Science Foundation of China (No. 21233004).

Notes and references

- H. Kim, G. Jeong, Y. U. Kim, J. H. Kim, C. M. Park, H. J. Sohn, *Chem. Soc. Rev.*, 2013, **42**, 9011–9034.
- A. Zhamu, G. Chen, C. Liu, D. Neff, Q. Fang, Z. Yu, W. Xiong, Y. Wang, X. Wang, B. Z. Jang, *Energy Environ. Sci.*, 2012, **5**, 5701–5707.
- X. Ji, K. T. Lee, L. F. Nazar, *Nat. Mater.*, 2009, **8**, 500–506.
- X. Ji, L. F. Nazar, *J. Mater. Chem.*, 2010, **20**, 9821–9826.
- P. G. Bruce, S. A. Freunberger, L. J. Hardwick, J.-M. Tarascon, *Nat. Mater.*, 2012, **11**, 19–29.
- Y. Shao, F. Ding, J. Xiao, J. Zhang, W. Xu, S. Park, J. -G. Zhang, Y. Wang, J. Liu, *Adv. Funct. Mater.*, 2013, **23**, 987–1004.
- G. Girishkumar, B. McCloskey, A. C. Luntz, S. Swanson, W. Wilcke, *J. Phys. Chem. Lett.*, 2010, **1**, 2193–2203.
- J. -S. Lee, S. T. Kim, R. Cao, N. -S. Choi, M. Liu, K. T. Lee, J. Cho, *Adv. Energy Mater.*, 2011, **1**, 34–50.
- K. Yoshimura, J. Suzuki, K. Sekine, T. Takamura, *J. Power Sources*, 2005, **146**, 445–447.
- Y. V. Mikhaylik, J. R. Akridge, *J. Electrochem. Soc.*, 2003, **150**, A306–A311.
- F. B. Dias, L. Plomp, J. B. J. Veldhuis, *J. Power Sources*, 2000, **88**, 169–191.
- A. M. Stephan, *Eur. Polym. J.*, 2006, **42**, 21–42.

- 13 C. Naudin, J. L. Bruneel, M. Chami, B. Desbat, J. Grondin, J. C. Lassègues, L. Servant, *J. Power Sources*, 2003, **124**, 518–525.
- 14 P. L. Moss, R. Fu, G. Au, E. J. Plichta, Y. Xin, J. P. Zheng, *J. Power Sources*, 2003, **124**, 261–265.
- 15 S. Chandrashekar, N. M. Trease, H. J. Chang, L. -S. Du, C. P. Grey, A. Jerschow, *Nat. Mater.*, 2012, **11**, 311–315.
- 16 D. Aurbach, E. Zinigrad, H. Teller, P. Dan, *J. Electrochem. Soc.*, 2000, **147**, 1274–1279.
- 17 Y. Zhang, J. Qian, W. Xu, S. M. Russell, X. Chen, E. Nasybulin, P. Bhattacharya, M. H. Engelhard, D. Mei, R. Cao, F. Ding, A. V. Cresce, K. Xu, J. G. Zhang, *Nano Lett.*, 2014, **14**, 6889–6896.
- 18 H. Ota, X. Wang, E. Yasukawa, *J. Electrochem. Soc.*, 2004, **151**, A427–A436.
- 19 R. Mogi, M. Inaba, S. -K. Jeong, Y. Iriyama, T. Abe, Z. Ogumi, *J. Electrochem. Soc.*, 2002, **149**, 1578–1583.
- 20 Y. Matsuda, *J. Power Sources*, 1993, **43**, 1–7.
- 21 Z. Li, J. Huang, Bor Yann Liaw, Viktor Metzler, J. Zhang, *J. Power Sources*, 2014, **254**, 168–182.
- 22 W. Xu, J. Wang, F. Ding, X. Chen, E. Nasybulin, Y. Zhang, J. -G. Zhang, *Energy Environ. Sci.*, 2014, **7**, 513–537.
- 23 H. -C. Shin, M. Liu, *Adv. Funct. Mater.*, 2005, **15**, 582–586.
- 24 J. Hassoun, S. Panero, P. Simon, P. L. Taberna, B. Scrosati, *Adv. Mater.*, 2007, **19**, 1632–1635.
- 25 H. Kim, B. Park, H. -J. Sohn, T. Kang, *J. Power Sources*, 2000, **90**, 59–63.
- 26 W. X. Chen, J. Y. Lee, Z. Liu, *Carbon*, 2003, **41**, 959–966.
- 27 Z. Chen, J. Qian, X. Ai, Y. Cao, H. Yang, *Electrochim. Acta*, 2009, **54**, 4118–4122.
- 28 J. H. Ryu, J. W. Kim, Y. E. Sung, S. M. Oh, *Electrochem. Solid-State Lett.*, 2004, **7**, A306–A309.
- 29 L. Balan, R. Schneider, J. Ghanbaja, P. Willmann, D. Billaud, *Electrochim. Acta*, 2006, **51**, 3385–3390.
- 30 A. Dailly, R. Schneider, D. Billaud, Y. Fort, P. Willmann, *Electrochim. Acta*, 2002, **47**, 4207–4212.
- 31 D. Billaud, C. Nabais, C. Mercier, R. Schneider, P. Willmann, *Energy Convers. Manage.*, 2008, **49**, 2447–2454.
- 32 A. Anani, R. A. Huggins, *J. Power Sources*, 1992, **38**, 363–372.
- 33 M. Winter, J. O. Besenhard, *Electrochimica Acta*, 1999, **45**, 31–50.
- 34 J. L. Barton, J. O'M. Bockris, *Proc. R. Soc. Lond*, 1962, **268**, 485–505.
- 35 J. W. Diggle, A. R. Despic, J. O'M. Bockris, *J. Electrochem. Soc.*, 1969, **112**, 1503–1514.
- 36 C. Monroe, J. Newman, *J. Electrochem. Soc.*, 2003, **150**, A1377–A1384.
- 37 C. Monroe, J. Newman, *J. Electrochem. Soc.*, 2004, **151**, A880–A886.
- 38 R. F. Voss, M. Tomkiewicz, *J. Electrochem. Soc.*, 1985, **132**, 371–375.
- 39 G. Nagy, Y. Sugimoto, G. Denuault, *J. Electroanal. Chem.*, 1997, **433**, 167–173.
- 40 R. V. Magan, R. Sureshkumar, B. Lin, *J. Phys. Chem.*, 2003, **107**, 10513–10520.
- 41 R. V. Magan, R. Sureshkumar, *Nanotechnology*, 2005, **16**, 545–553.
- 42 M. Z. Mayers, J. W. Kaminski, T. F. Miller, *J. Phys. Chem. C.*, 2012, **116**, 26214–26221.
- 43 J. -N. Chazalviel, *Phys. Rev. A*, 1990, **42**, 7355–7367.
- 44 C. Brissot, M. Rosso, J. -N. Chazalviel, S. Lascaud, *J. Power Sources*, 1999, **81**, 925–929.
- 45 M. Rosso, T. Gobron, C. Brissot, J. -N. Chazalviel, S. Lascaud, *J. Power Sources*, 2001, **97-98**, 804–806.
- 46 M. Rosso, E. Chassaing, J. -N. Chazalviel, T. Gobron, *Electrochim. Acta*, 2002, **47**, 1267–1273.
- 47 M. Rosso, C. Brissot, A. Teyssot, M. Dollé, L. Sannier, J. -M. Tarascon, R. Bouchet, S. Lascaud, *Electrochim. Acta*, 2006, **51**, 5334–5340.
- 48 J. Yamaki, S. Tobishima, K. Hayashi, K. Saito, Y. Nemoto, M. Arakawa, *J. Power Sources*, 1998, **74**, 219–227.
- 49 J. Zhu, Y. K. Sharma, Z. Zeng, X. Zhang, M. Srinivasan, S. Mhaisalkar, H. Zhang, H. H. Hng, Q. Yan, *J. Phys. Chem. C*, 2011, **115**, 8400–8406.